A convenient synthesis, in silico study and crystal structure of novel sulfamidophosphonates: Interaction with SARS-CoV-2

Rayenne Redjemia, Malika Berredjem, Ali Dekir, Malika Ibrahim-Ouali,
Sofiane Bouacida, Abdeslem Bouzina, Rania Bahadi

A convenient synthesis, in silico study and crystal structure of novel sulfamidophosphonates: Interaction with SARS-CoV-2

Rayenne Redjemia [a], Malika Berredjem [a,#,*], Ali Dekir [a], Malika Ibrahim-Ouali [b,#,*], Mohamed Aissaoui [a], Sofiane Bouacida [c], Abdeslem Bouzina [a], Rania Bahadi [a]

[a] Laboratoire de Chimie Organique Appliquée (LCOA), Groupe de Synthèse de Biomolécules et Modélisation Moléculaire, Université Badji-Mokhtar Annaba, BP 12, 23000 Annaba, Algérie
[b] Aix Marseille Univ, CNRS, Centrale Marseille, iSm2, Marseille, France
[c] Département Sciences de la Matière, Université Oum El Bouaghi, 04000 Oum El Bouaghi, Algérie and Unité de Recherche de Chimie de l'Environnement et Moléculaire Structurale, Université Frères Mentouri Constantine 25000, Algérie

article info

abstract

A one-pot synthetic strategy was developed for the synthesis of novel sulfamidophosphonates via a three-component Kabachnik-Fields reaction of sulfanilamide, triethyl phosphite, and various aldehyde using ultrasound irradiation. Seven organophosphorus derivatives were synthesized with high yields through this newly developed method. The target compounds were characterized by ^{1}H, ^{31}P, ^{13}C NMR, and IR. The molecular structure of **4a** was obtained by X-ray diffraction on the monocrystal. Crystal belongs to the orthorhombic system with space groups Pbca. Insight into the binding mode of the synthesized compounds (ligand) into the binding sites of SARS-CoV2 (PDF code: **5R80**) was provided by docking studies, performed with the help of Maestro 9.0 docking software.

© 2022 Elsevier B.V. All rights reserved.

1. Introduction

There are two main strategies for the discovery of new drugs based on two main strategies; either by structural modification of a drug molecule that already exists or by design and synthesis of an original molecule with a synergistic effect of two or more pharmacophores [1,2]. In recent years, biologists have reported human pathogens that are resistant to existing antibacterial drugs, for example; methicillin-resistant *Staphylococcus aureus* [3], vancomycin-resistant *enterococci* [4], and azole-resistant *Candida species* [5]. It is really difficult to cure infections caused by these microbes, especially in immunocompromised patients [6].

Inhibition of many target enzymes of resistant bacteria is an emerging strategy for developing new antibacterial drugs. Among the bioactive molecules described in the literature, some sulfonamide derivatives have shown promising antibacterial activities

[7–9]. Many sulfonamide derivatives were designed and synthesized as isosteres of carboxylic acids.

The combination of two pharmacophores such as sulfonamide and phosphonate is still the subject of research today in the medical field (Fig. 1), such as compound **1**, which exhibited applicative inhibitory activity of cyclooxygenase COX-2 (IC50= 0.28 µM) and antiproliferative capacity against several cancer cell lines [10]. Verma et al. [11] reported the synthesis of sulfonamidophosphonates **2**, the obtained results showed that they are good corrosion inhibitors for mild steel and their inhibition efficiency increases with the concentration. Furthermore, new sulfonamidophosphonates have been developed as selective inhibitors of COX-2 (the mediator of cell survival, proliferation, and apoptosis) and anticancer candidates. Compounds **3**, **4**, and **5** were evaluated for their in vitro antituberculous activity against Mycobacterium tuberculosis H37Rv. These compounds exhibited superior antituberculosis activity compared to standard drugs; ethambutol and pyrazinamide with a minimum inhibitory concentration MIC value of 1.56 µg/mL. (Fig. 2) [12].

Currently, viral infections are the source of many diseases affecting the whole world, and we are constantly seeing the appearance of new ones. This is seen with the epidemic of severe acute

* Corresponding authors.
E-mail addresses: malika.berredjem@univ-annaba.org (M. Berredjem), malika.ibrahim@univ-amu.fr (M. Ibrahim-Ouali).
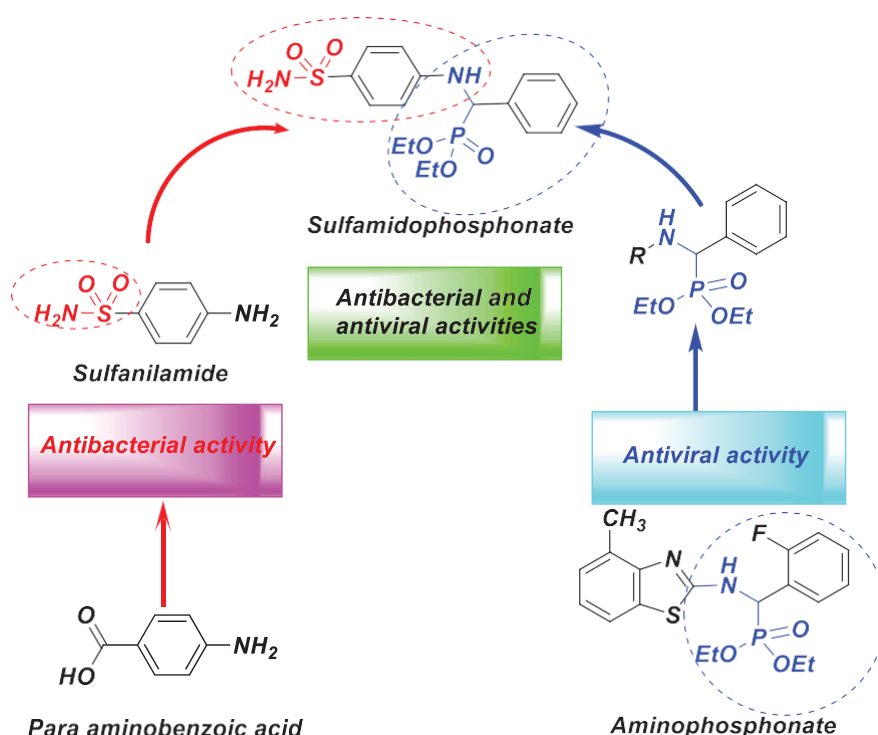# Participated equally in this collaborative work.

Fig. 1. Rational approach to the design of active compounds containing sulfonamide and phosphonate moieties.
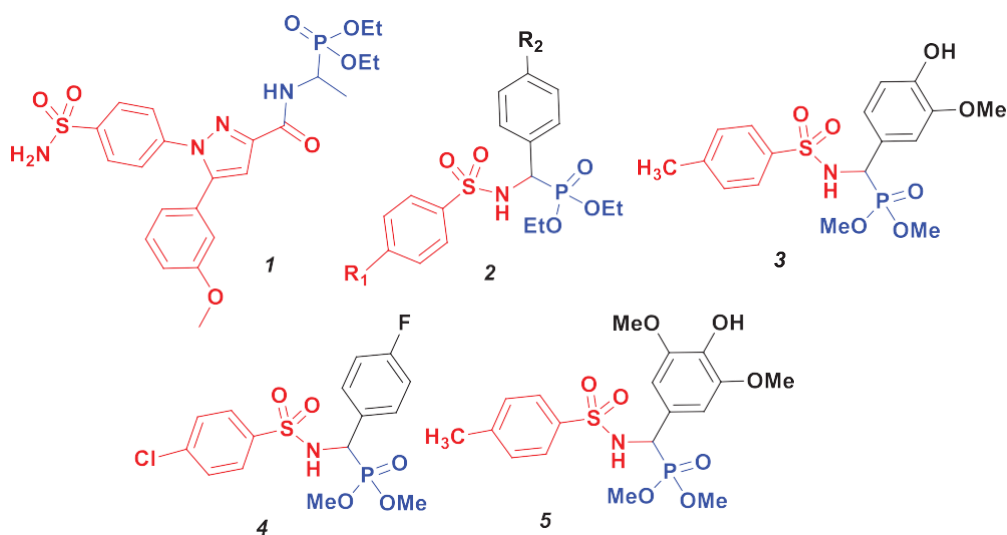

Fig. 2. Structures of sulfamidophosphonates having biological activities.

respiratory syndrome (SARS) or even more recently with the coronavirus disease 2019 (COVID −19) [13,14]. Virtual screening is a technique developed by researchers to design new biomolecules against the coronavirus [15–18]. The main protease enzyme (M^{pro}) is essential for viral replication and has been considered as one of the potent drug targets for treating COVID-19. The functional role of M^{pro} in the viral replication highlights its importance that can be used to identify the potential drug therapeutics against COVID-19.

In silico simulations have identified new compounds with potential antiviral activity, which require further experimental studies. Sulfonamides and phosphonates are known for their remarkable antiviral activities [19,20].

We have presented a novel and simple route to the successful synthesis of seven novel sulfamidophosphonates, which were then subjected to X-ray diffraction. Next, its antiviral potency against SARS-CoV-2 Mpro was tested using Autodock and Maestro to compare its antiviral performance with various synthetic drugs.

The new single crystals were obtained by recrystallizing from ethanol of the products named **diethyl (phenyl((4-sulfamoylphenyl)amino)methyl)phosphonate (3a)**. A search in the CSD database version 5.41 using the ConQuest software version 2020.1 for molecules with the same core did not generate any results about its crystallographic analysis. Therefore, we report a complete study on the molecular and supramolecular structures.

The crystal was kept at 295 K during data collection. Using Olex2 [21], the structure was solved with the SHELXT [22] structure solution program using Intrinsic Phasing and refined with the SHELXL [23] refinement package using Least Squares minimisation.

2. Experimental section

2.1. General information

The chemicals used in this work were obtained from Fluka and Merck Chemical Company and were used without purification.

All reactions were monitored by TLC on silica Merck 60 F$_{254}$ percolated aluminum plates and were developed by spraying with ninhydrin solution. Sonication was performed in a FUNGILAB ultrasonic bath with a frequency of 40 kHz and output power of 250 W. The reactions were carried out in an open glass tube (diameter: 25 mm; thickness: 1 mm; volume: 20 cm^3) at room temperature. IR spectra were recorded as KBr pellets on a Perkin Elmer 781 spectrophotometer and an Impact 400 Nicolet FT-IR spectrophotometer. ^{1}H NMR and ^{13}C NMR and ^{31}P NMR spectra were recorded on a Bruker spectrometer at 400 MHz using tetramethylsilane (TMS) as internal standard and DMSO–d6 or CDCl$_3$ as solvent. Chemical shifts are reported in δ units (ppm) with TMS as reference (δ 0.00). All coupling constants (*J*) are reported in Hertz. Multiplicity is indicated by one or more of the following: s (singlet), d (doublet), dd (doublet of doublet), t (triplet), td (triplet of doublet), q (quartet), m (multiplet).

Melting points were measured in open capillary tubes on an electrothermal apparatus and uncorrected.

2.2. General procedure for the synthesis of sulfamidophosphonate derivatives 3(a-g)

In a 10 mL round bottom flask taken a mixture of sulfanilamide (1 mmol) aldehyde (1 mmol) and at room temperature and then triethyl phosphite (1 mmol) was added. The reaction mixture was then sonicated by an ultrasonic bath at a frequency of 40 kHz for 10 to 15 min. After completion of the reaction, as indicated by TLC, silica gel dichloromethane- methanol (99/1). The final product was purified by column chromatography eluted dichloromethane-methanol (99/1) or was crystallized in diethyl ether/n-hexane, and the mixture was cooled to 6 °C overnight. The product was finally filtered and dried to afford the pure α-sulfamidophosphonates in excellent yields.

2.3. Spectral data

2.3.1. Diethyl (phenyl((4-sulfamoylphenyl)amino)methyl)phosphonate (4a)

White powder, yield 88%, m.p. 198–200 °C, Rf =0.22 (CH$_2$Cl$_2$/MeOH: 96/4)^{1}H NMR (400 MHz, DMSO–d6) δ 7.54–7.52 (m, 2H, H$_{Ar}$) 7.44(d, *J*=8.8 Hz, 2H, NH$_2$) 7.33(t, *J* = 12 Hz, 2H, H$_{Ar}$) 7.26–7.23 (m, 1H, NH), 7.09–7.05 (m,1H, H$_{Ar}$), 6.89(d, *J* = 8.8 Hz, 4H, H$_{Ar}$), 5.15 (dd, 1H, *CH), 4.08–4.00 (m, 1H, CH$_2$), 3.92–3.86 (m, 1H, CH$_2$), 3.76–3.72 (m, 1H, CH$_2$), 1.18(t, *J* = 7 Hz, 3H, CH$_3$), 1.05 (t, *J* = 7 Hz, 3H, CH$_3$) ppm. ^{13}C NMR (101 MHz, DMSO) δ 150.09 (d, *J* = 13.4 Hz), 136.26, 131.51, 128.24 (d, *J* = 5.4 Hz), 128.01 (d, *J* = 2.4 Hz), 127.49 (d, *J* = 2.9 Hz), 126.91, 112.36, 62.49 (d, J_{c-p} = 6.8 Hz, <u>CH$_2$</u>–CH$_3$), 62.30(d, J_{c-p} = 6.9 Hz, <u>CH$_2$</u>–CH$_3$), 53.44 (*J*$_{c-p}$ = 151.2, *CH), 16.25 (d, J_{c-p} = 5.2 Hz, CH$_2$–<u>CH$_3$</u>), 16.00 (d, J_{c-p} = 5.4 Hz, CH$_2$–<u>CH$_3$</u>), ppm. ^{31}P NMR (100 MHz, DMSO–d6) δ 22.19 ppm. IR (KBr, cm^{-1}): 3342.05 (NH$_2$), 1149.70–1319.94 (SO$_2$), 1227.04 (P=O). Anal. Calcd for C$_{17}$H$_{23}$N$_2$O$_5$PS C, 51.25; H, 5.82; N, 7.03. Found: C, 51.30; H, 5.70; N, 7.10.

2.3.2. Diethyl ((4-fluorophenyl)((4-sulfamoylphenyl)amino)methyl) phosphonate (4b)

Yellow powder , yield: 86% , m.p 168–170 °C , Rf =0.22 (CH$_2$Cl$_2$/MeOH: 96/4)^{1}H NMR (400 MHz, DMSO–d6) δ 7.56 (ddd, *J* = 7.6, 5.4, 2.2 Hz, 2H, H$_{Ar}$), 7.45 (d, *J* = 7.1 Hz, 2H, NH$_2$), 7.20 – 7.04 (m, 3H, H$_{Ar}$), 6.93–6.85 (m, 4H, H$_{Ar}$), 5.20 (dd, 1H,

*CH), 4.04 (dqd, *J* = 11.2, 7.0, 2.8 Hz, 2H, CH$_2$), 3.95 – 3.87 (m, 1H, CH$_2$), 3.82 – 3.73 (m, 1H, CH$_2$), 1.17 (t, *J* = 7.0 Hz, 3H, CH$_3$), 1.06 (t, *J* = 7.1 Hz, 3H, CH$_3$) ppm. ^{13}C NMR (101 MHz, DMSO–d6) δ 162.95, 160.53, 150.09 (d, *J*=13.5 Hz), 132.58 (d, *J* = 2.9 Hz), 131.74, 130.38–130.25(m), 127.11, 115.17–114.93(m), 62.81 (d, J_{c-p} = 6.6 Hz, <u>CH$_2$</u>–CH$_3$), 62.57 (d, J_{c-p} = 6.9 Hz, <u>CH$_2$</u>–CH$_3$), 52.75 (d, J_{c-p} = 152 Hz,*CH) 16.35 (d, J_{c-p} = 5.1 Hz, CH$_2$–<u>CH$_3$</u>), 16.15(4, J_{c-p} = 5.5 Hz, CH$_2$–<u>CH$_3$</u>) ppm. IR (KBr, cm^{-1}): 3332.54 (NH$_2$), 1149.16–1318.92 (SO$_2$), 1225.03 (P=O). Anal. Calcd for C$_{17}$H$_{22}$FN$_2$O$_5$PS: C, 49.04; H, 5.33; N, 6.73. Found: C, 49.15; H, 5.40; N, 6.80.

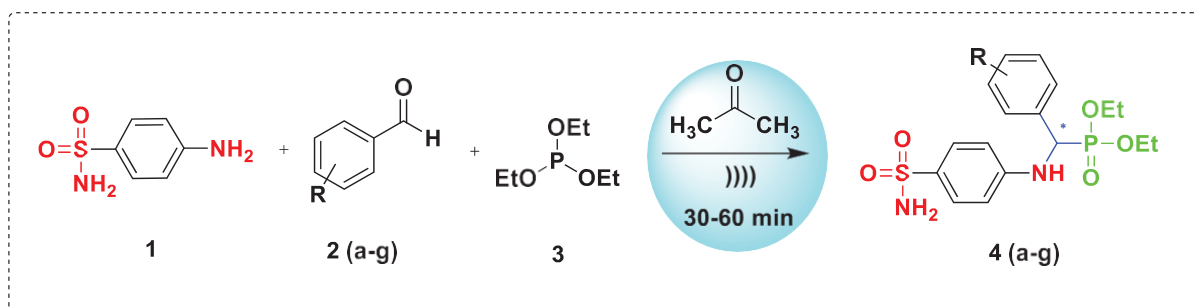#### 2.3.3. Diethyl ((4-bromophenyl)((4-sulfamoylphenyl)amino)methyl) phosphonate (4c)

White powder, yield 80%, m.p. 172–174 °C, Rf =0.24 (CH$_2$Cl$_2$/MeOH: 96/4) ^{1}H NMR (400 MHz, DMSO–d6) δ 7.54 (dd, *J* = 8.6, 2.2 Hz, 2H, H$_{Ar}$), 7.46 (d, *J* = 8.9 Hz, 2H, NH$_2$), 7.40 (d, *J* = 8.4 Hz, 2H, H$_{Ar}$), 7.07 (dd, *J* = 9.7, 6.6 Hz, 1H, NH), 6.95 – 6.81 (m, 4H, H$_{Ar}$), 5.20 (dd, 1H, *CH), 4.12 – 3.99 (m, 2H, CH$_2$), 3.98 – 3.87 (m, 1H, CH$_2$), 3.87 – 3.74 (m, 1H, CH$_2$), 1.18 (t, *J* = 7.0 Hz, 3H, CH$_3$), 1.08 (t, *J* = 7.1 Hz, 3H, CH$_3$) ppm. ^{13}C NMR (101 MHz, DMSO–d6) δ 150.02 (d, *J* = 13.4 Hz), 135.54, 132.34 (d, *J* = 3.6 Hz), 131.80 (d, *J* = 5.5 Hz), 128.19 (d, *J* = 2.5 Hz), 127.09, 62.85 (d, J_{c-p} = 6.9 Hz, <u>CH$_2$</u>–CH$_3$), 62.59 (d, J_{c-p} = 6.9 Hz, <u>CH$_2$</u>–CH$_3$), 52.87 (d, J_{c-p} = 151.3 Hz, *CH), 16.35 (d, J_{c-p} = 5.1 Hz, CH$_2$–<u>CH$_3$</u>), 16.15 (d, J_{c-p} = 5.5 Hz, CH$_2$–<u>CH$_3$</u>) ppm. IR (KBr, cm^{-1}): 3351.92 (NH$_2$), 1150.03–1322.47 (SO$_2$), 1225.53 (P=O). Anal. Calcd for C$_{17}$H$_{22}$BrN$_2$O$_5$PS C, 42.78; H, 4.65; N, 5.87. Found : C, 42.85; H, 4.57; N, 5.77.

2.3.4. Diethyl ((4-methoxyphenyl)((4-sulfamoylphenyl)amino)methyl) phosphonate (4d)

White powder, yield 85%, m.p. 158–160 °C, Rf = 0.22 (CH$_2$Cl$_2$/MeOH: 96/4). ^{1}H NMR (400 MHz, DMSO–d6) δ 7.44 (dd, *J* = 8.9, 2.0 Hz, 4H, NH$_2$+H$_{Ar}$), 7.02 (dd, *J* = 9.8, 6.4 Hz, 1H, NH), 6.95 – 6.77 (m, 6H, H$_{Ar}$), 5.15 (dd, 1H, *CH), 4.14–3.94 (m, 2H, CH$_2$), 3.94 – 3.82 (m, 1H, CH$_2$), 3.78–3.73 (m, 1H, CH$_2$),3.72 (s, 3H, OCH$_3$), 1.18 (t, *J* = 7.0 Hz, 3H, CH$_3$), 1.07 (t, *J* = 7.0 Hz, 3H, CH$_3$) ppm.^{13}C NMR (101 MHz, DMSO–d6) δ 158.68 (d, *J* = 2.9 Hz), 150.15 (d, *J* = 13.4 Hz), 131.42, 129.43 (d, *J* = 5.5 Hz), 127.949, 126.902, 113.51 (d, *J* = 2.1 Hz), 112.40, 62.42 (d, J_{c-p} = 7 Hz, <u>CH$_2$</u>–CH$_3$), 62.27 (d, J_{c-p} = 6.9 Hz, <u>CH$_2$</u>–CH$_3$), 54.26 (d, J_{c-p} = 150.6 Hz, *CH), 16.30 (d, J_{c-p} = 5.5 Hz, CH$_2$–<u>CH$_3$</u>), 16.09 (d, J_{c-p} = 5.5 Hz,CH$_2$–<u>CH$_3$</u>) ppm. IR (KBr, cm^{-1}): 3317.19 (NH$_2$), 1153.18–1310.95 (SO$_2$), 1223.14 (P=O).Anal.Calcd for C$_{18}$H$_{25}$N$_2$O$_6$PS C, 50.46; H, 5.88; N, 6.54. Found: C, 50.51; H, 5.80; N, 6.62.

2.3.5. Diethyl ((4-hydroxyphenyl)((4-sulfamoylphenyl)amino)methyl) phosphonate (4e)

White powder, yield 84%, m.p. 90–92 °C, Rf = 0.11 (CH$_2$Cl$_2$/MeOH: 96/4). ^{1}H NMR (400 MHz, DMSO–d6) δ 9.38 (s, 1H, OH), 7.45 (d, *J* = 8.9 Hz, 2H, NH$_2$), 7.32 (dd, *J* = 8.7, 2.2 Hz, 2H, H$_{Ar}$), 6.97 (dd, *J* = 9.8, 6.2 Hz, 1H, NH), 6.92–6.84 (m, 4H, H$_{Ar}$), 6.71 (d, *J* = 8.6 Hz, 2H), 5.0 (dd, 1H, *CH), 4.06 – 4.00 (m, 2H, CH$_2$), 3.88 (dt, *J* = 10.3, 7.2 Hz, 1H, CH$_2$), 3.76 – 3.67 (m, 1H, CH$_2$), 1.18 (t, *J* = 7.0 Hz, 3H, CH$_3$), 1.06 (t, *J* = 7.0 Hz, 3H, CH$_3$) ppm.^{13}C NMR (101 MHz, DMSO–d6) δ 156.54 (d, *J* = 2.6 Hz), 150.21 (d, *J* = 13.5 Hz), 131.32, 129.42 (d, *J* = 5.8 Hz), 126.91, 126.10, 114.89 (d, *J* = 2.2 Hz), 112.36, 62.30 (d, J_{c-p} = 13.4 Hz, <u>CH$_2$</u>–CH$_3$), 61.17 (d, J_{c-p} = 5.5 Hz, <u>CH$_2$</u>–CH$_3$), 52.86(d, J_{c-p} = 153.1 Hz, *CH), 16.31 (d, J_{c-p} = 5.1 Hz, CH$_2$–<u>CH$_3$</u>), 16.09 (d, J_{c-p} = 5.1 Hz, CH$_2$–<u>CH$_3$</u>) ppm. IR (KBr, cm^{-1}): 3343.79 (NH$_2$), 1147.64–1323.66 (SO$_2$), 1219.42 (P=O). Anal. Calcd for C$_{17}$H$_{23}$N$_2$O$_6$PS: C, 49.27; H, 5.59; N, 6.76. Found: C, 49.35; H, 5.67; N, 6.84.

Scheme 1. Synthesis of α-sulfamidophosphonate derivatives.

2.3.6. Diethyl (((4-sulfamoylphenyl)amino)(m-tolyl)methyl) phosphonate (4f)

White powder, yield 86%, m.p. 194–196 °C, Rf = 0.21 (CH$_2$Cl$_2$/MeOH: 96/4). **^{1}H NMR** (400 MHz, DMSO–d6) δ 7.48–7.42 (m, 2H, NH$_2$), 7.38 − 7.30 (m, 2H, H$_{Ar}$), 7.21 (t, J = 7.6 Hz, 1H, NH), 7.13 − 7.01 (m, 2H, H$_{Ar}$), 6.94 − 6.83 (m, 4H, H$_{Ar}$), 5.10 (dd, 1H, *CH), 4.12 − 3.98 (m, 2H, CH$_2$), 3.94 − 3.82 (m, 1H, CH$_2$), 3.78 − 3.64 (m, 1H, CH$_2$), 2.28 (s, 3H, CH$_3$), 1.18 (t, J = 7.0 Hz, 3H, CH$_3$), 1.06 (t, J = 7.0 Hz, 3H, CH$_3$) ppm. **^{13}C NMR** (101 MHz, DMSO–d6) δ 150.17 (d, J = 13.5 Hz), 137.09 (d, J = 2.6 Hz), 136.21, 131.47, 128.81 (d, J = 5.5 Hz), 128.24, 127.94, 127.41, 126.96, 125.43 (d, J = 5.4 Hz), 62.51 (d, J_{c-p} = 6.9 Hz, CH$_2$–CH$_3$), 62.36 (d, J_{c-p} = 6.9 Hz, CH$_2$–CH$_3$), 53.38 (d, J_{c-p} = 151 Hz, *CH), 16.30 (d, J_{c-p} = 5.1 Hz, CH$_2$–CH$_3$), 16.03 (d, J_{c-p} = 5.8 Hz, CH$_2$–CH$_3$) ppm. **IR** (KBr, cm^{-1}): 3336.3 (NH), 1149.46–1315.53 (SO$_2$), 1208.35 (P=O).

Anal. Calcd for C$_{18}$H$_{25}$N$_2$O$_5$PS: C, 52.42; H, 6.11; N, 6.79. Found: C, 52.54; H, 6.21; N, 6.87.

2.3.7. Diethyl ((4-chlorophenyl)((4-sulfamoylphenyl)amino)methyl) phosphonate (4g)

White powder, yield 79%, m.p.178–180 °C, Rf = 0.20 (CH$_2$Cl$_2$/MeOH: 96/4). **^{1}H NMR** (400 MHz, DMSO–d6) δ 7.66 (d, J = 7.5 Hz, 1H, NH), 7.53–7.42 (m, 3H, NH$_2$+H$_{Ar}$), 7.38 − 7.22 (m, 3H, H$_{Ar}$), 6.92 (s, 2H, H$_{Ar}$), 6.76 (d, J = 8.9 Hz, 2H, H$_{Ar}$), 5.30 (dd, 1H, *CH), 4.11 (m, 2H, CH$_2$), 3.88 (dt, J = 10.5, 7.5 Hz, 1H, CH$_2$), 3.78 − 3.63 (m, 1H, CH$_2$), 1.22 (t, J = 7.0 Hz, 3H, CH$_3$), 1.02 (t, J = 7.0 Hz, 3H, CH$_3$) ppm. **^{13}C NMR** (101 MHz, DMSO–d6) δ 149.61 (d, J = 13.9 Hz), 133.93, 133.38 (d, J = 7.7 Hz), 132.17, 129.60, 129.16, 127.36, 112.11, 62.94 (d, J_{c-p} = 6.9 Hz, CH$_2$–CH$_3$), 62.67 (d, J_{c-p} = 6.9 Hz, CH$_2$–CH$_3$), 50.51 (d, J_{c-p} = 155 Hz, *CH), 16.30 (d, J_{c-p} = 5.5 Hz, CH$_2$–CH$_3$), 15.94 (d, J_{c-p} = 5.1 Hz, CH$_2$–CH$_3$) ppm. **IR** (KBr, cm^{-1}): 3286.65 (NH$_2$) 1148.98–1327.16(SO$_2$), 1205.50 (P=O). Anal. Calcd for C$_{17}$H$_{22}$ClN$_2$O$_5$PS: C, 47.17; H, 5.12; N, 6.47. Found: C, 47.25; H, 5.08; N, 6.55.

3. Results and discussion

3.1. Synthesis and characterization

The application of ultrasound as a catalyst in chemical synthesis has become an important field of research.

Herein, to continue the previous work of our group on phosphonate and sulfonamide derivatives [24–29], we are interested to study the one-pot synthesis of α-sulfamidophosphonate under a green, clean, and environment-friendly method using ultrasound irradiation. In this work sulfanilamide **1** was reacted with various aromatic aldehydes (**2a**-2 g) and triethyl phosphite in the absence of any catalyst after 30–60 min, the reaction was completed with an excellent yields (Scheme 1).

Scheme 2

Table 1
Optimization of reaction time and solvent for the synthesis of α-sulfamidophosphonates.

Entry	Solvent	Time/min	Temp/ °C	Yields%
1	No solvent	90	r.t	—
2	CH$_2$Cl$_2$	90	r.t	—
3	MeOH	75	r.t	40
4	EtOH	60	r.t	50
5	Acetone	30	r.t	90

At room temperature, some solvents were examined under ultrasound irradiation, and it is observed that the reaction formed only a low yield in CH$_2$Cl$_2$, MeOH, and EtOH.

A higher yield of 90% was obtained using acetone as solvent (Table 1).

The reaction between sulfanilamide **1**, benzaldehyde, and triethyl phosphite was selected as a model to evaluate the feasibility of α-sulfamidophosphonates and to optimize the reaction conditions.

3.2. Mechanistic proposal

The structures of the synthesized compounds are confirmed by elemental analysis as well as by IR and ^{1}H, ^{13}C, and ^{31}P NMR spectral data. The ^{31}P NMR spectrum of the **4a** exhibited one peak at δ = 22.19 ppm.

NMR spectra were recorded using DMSO as the solvent and are available in the supplementary material part. The ^{1}H spectrum always showed a deshielded doublet of doublets at δ= [5.0–5.30] ppm corresponding to the NH*CH(R)PO(OEt)$_2$. The two CH$_2$ groups of the mustard moiety appeared at δ = [4.14–3.87] and [3.94–3.63].

In the FT-IR spectrum, we observed an absorption band toward [3351.92- 3286.65] cm^{-1} corresponding to the NH group, the sulfamide group stretching with signals at [1153.18–1147.64] cm^{-1} and [1327.16–1310.95] cm^{-1} and the phosphonate group appear around [1229.42–1205.92] cm^{-1}.

In ^{13}C spectrum was also characteristic due to the expected doublets related to the presence of the phosphorus (J_{C-P} couplings), the two ethoxy groups of the phosphonates appeared at [16.37–15.94] ppm (J_{C-P} ~ 5.1–5.8 Hz), [62.95–61.17] ppm (J_{C-P} ~ 6.6–7 Hz), and the asymmetric carbon NH*CH(R) PO(OEt)$_2$ at [50.51–54.26] ppm (doublet with a large coupling constant J_{C-P} ~150.6–155 Hz).

3.3. X-ray diffraction data and crystal structures of compounds 4a

Structural resolution of compound **3a** revealed that the asymmetric unit consists of one molecule of **diethyl (phenyl((4-sulfamoylphenyl)amino)methyl)phosphonate (4a)**, which crystallizes in orthorhombic system space groups Pbca (Table 1). The ORTEP diagram of this compound is shown in Fig. 3.
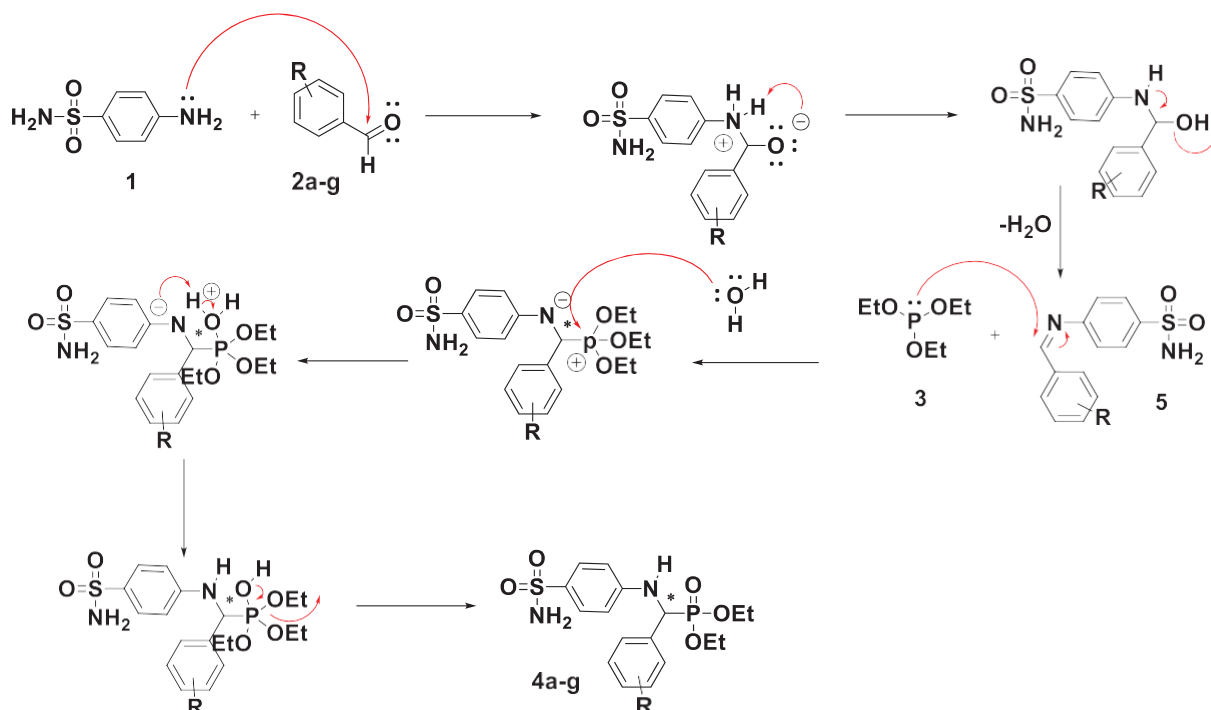
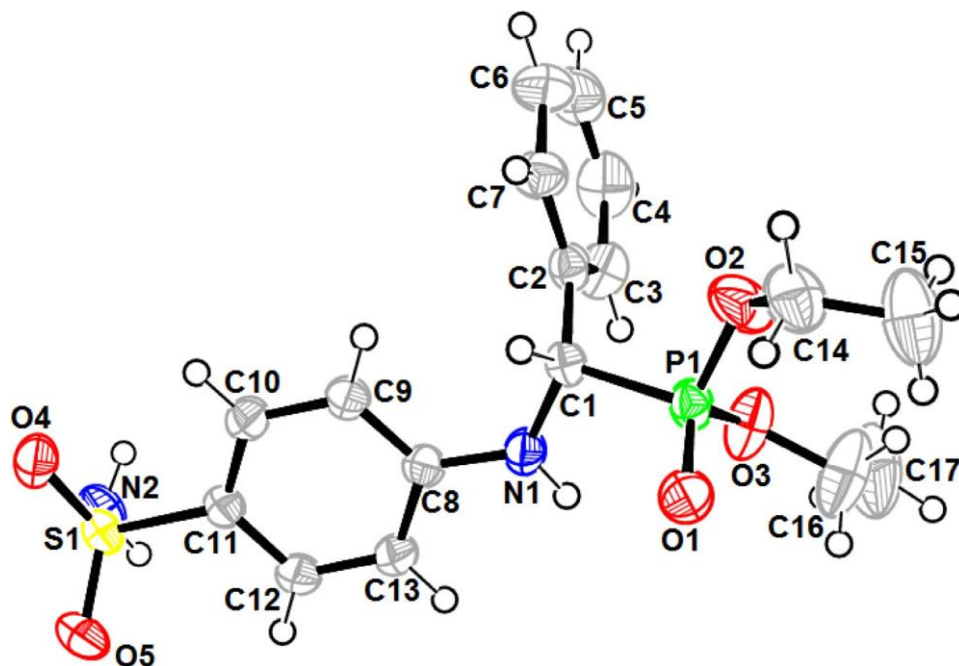**Scheme 2.** Mechanistic proposal for synthesis of the novel compounds.

Fig. 3. Ortep drawing of compound **4a** and its numbering scheme. Thermal ellipsoids were drawn at the 50% probability level.

The dihedral angle between the mean planes of the two phenyl rings is 81.01(2) °. The crystal packing can be described as alternating layers parallel to (001) plane along the c axis (Fig. 4) which are connected together with N−H…O and C−H…O hydrogen bonds (Table 2).

In these layers, the arrangement of each molecule induces a weak *П −П* staking intermolecular interactions. The shortest centroid–centroid distance is 5.3124(1)Å between phenyl rings.

Tables 3 and 4

The crystal structure is also supported by weak intermolecular interactions of C−H…*П* interactions (C14−H14a…Cg1 with Cg1: centroid of phenyl ring of (C2-C7).

The values of the selected interatomic distances (Å), valence angles (°) and torsion angles (°) of compound **4a** are represented in Tables 5–7.

3.4. Molecular docking

The protein structure of SARS-CoV-2 main protease (PDB ID: 5R80) was retrieved from the Protein Data Bank [30] and was prepared with the Protein Preparation Wizard tool implemented in the Schrodinger suite, assigning bond orders, adding hydrogens, and optimizing H-bonding networks. The three-dimensional structures of the derivatives were constructed using Maestro software

Table 2

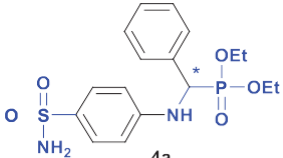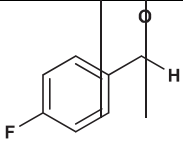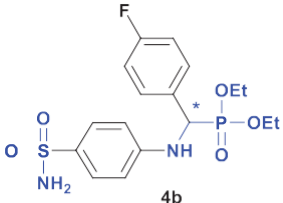Physico-chemical characterization of the new synthesized compounds **4a-4g**.
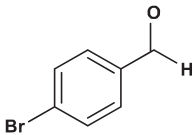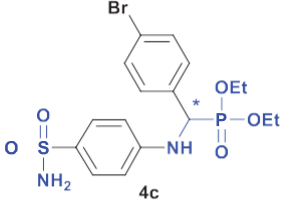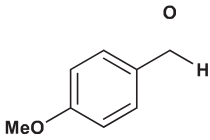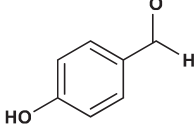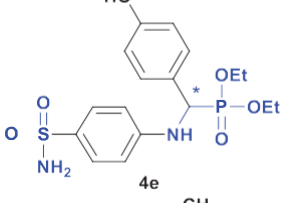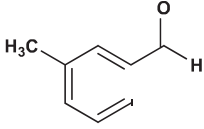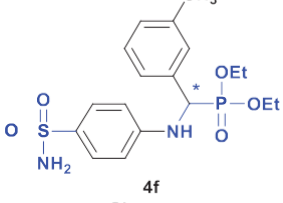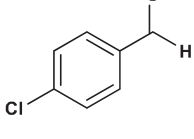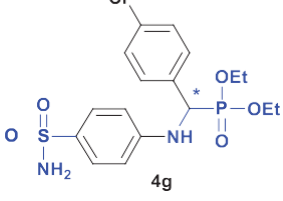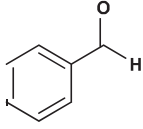
Entry	Aldehyde	Compound	Time	Yields%	Melting point °C
1	**4a**	**2b**	30	88	198–200
2	**4b**	**2c**	30	86	168–170
3	**4c**	**2d**	40	80	172–174
4	**4d**	**2e**	40	85	158–160
5	**4e**	**2f**	60	84	90–92
6	**4f**	**2g**	50	86	194–196
7	**4g**	**2a**	50	79	178–180

Table 3

Distances (Å) and angles (°) of hydrogen bond for **4a**.

D—H...A	d(D—H)	d(H...A)	d(D—A)	D—H—A	Symmetry
N1–H1...O4	0.86	0.2300	3.0081(1)	150.0	1/2 + x,y,1/2-z
N2–H2a...O1	0.89	2.0000	2.8783(1)	171.0	1/2-x,−1/2 + y,z
C13–H13...O1	093	2.5700	3.1758(1)	123.0	1-x,−1/2 + y,1/2-z
C13–H13...O4	0.93	2.5900	3.3143(1)	135.0	1/2 + x,y,1/2-z
C10–H10...O4	0.93	2.5700	2.9304(1)	104.0	x,y,z
C14–H14b...O1	0.97	2.5900	2.9961(1)	105.0	x,y,z

Fig. 4. The crystal packing of compound **4a**, viewed from b axis, showing a double layer along a c axis.
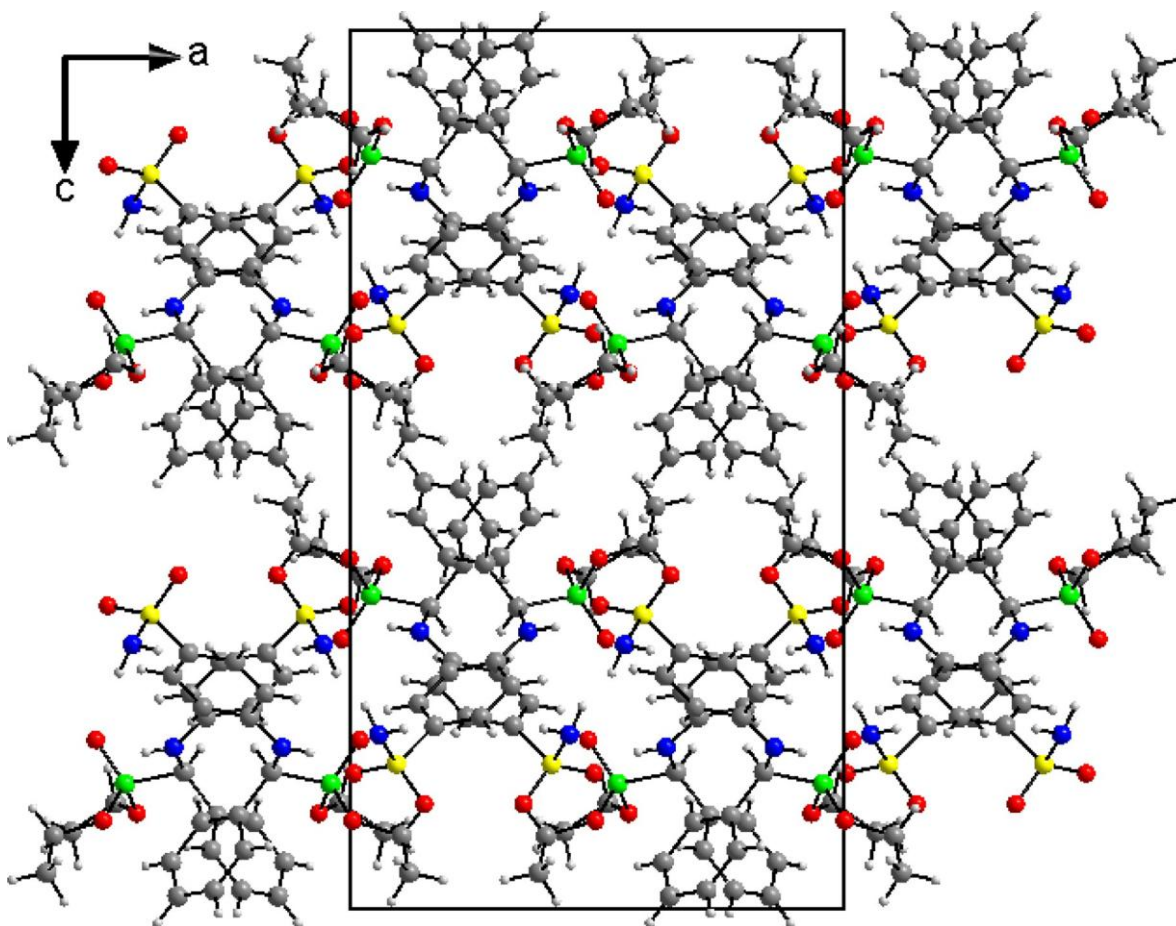
Table 4

Crystallographic data and refinement parameters for **4a**.

Crystal data	Compound **3a**
Chemical formula	$C_{17}H_{23}N_2O_5PS$
M_r	398.40
Crystal system, space group	Orthorhombic , Pbca
Temperature (K)	295
a, b, c (Å)	13.54695(11), 11.72156(9), 24.2554(2)
α (°), β (°), λ (°)	90
V (Å³)	3851.56(6)
Z	8
ρ_{calc} (g/cm³)	1.374
Radiation type	Cu κα (λ = 1.54184)
m (mm⁻¹)	
	2.546
Crystal size (mm)	0.46 × 0.16 × 0.1
Data collection	
Diffractometer	SuperNova, Dual, Cu at home/near, AtlasS2
Absorption correction	Multi-scan
T_{min}, T_{max}	0.441,1.000
2Θ range for data collection (°)	7.29 to 151.764
Index ranges	$-16 \le h \le 16$, $-14 \le k \le 14$, $-27 \le l \le 30$
Final R indexes [$I>=2\sigma$ (I)]	
	$R_1 = 0.0425$, $wR_2 = 0.1203$
Final R indexes [all data]	$R_1 = 0.0442$, $wR_2 = 0.1229$
Independent reflections	3995 [$R_{int} = 0.0321$, $R_{sigma} = 0.0208$]
Reflections collected	21,194
Refinement	
Goodness-of-fit on F²	1.025
Data/restraints/parameters	3995/0/238
Largest diff. peak/hole: Δ_{max}, Δ_{min} (e Å⁻³)	0.36/−0.33

Table 5

Selected interatomic distances (Å) and valence angles (°) of crystals **4a**.

Bonding atoms	Bond lengths (Å)	Bonding atoms	Bond lengths (Å)
S1—O4	1.4301(13)	C2—C7	1.380(2)
S1—O5	1.4288(12)	C3—C4	1.386(3)
S1—N2	1.6227(16)	C4—C5	1.376(4)
S1—C11	1.7570(15)	C5—C6	1.369(3)
P1—O1	1.4694(12)	C6—C7	1.394(3)
P1—O2	1.5535(14)	C8—C9	1.399(2)
P1—O3	1.5627(14)	C8—C13	1.406(2)
P1—C1	1.8232(15)	C9—C10	1.386(2)
O2—C14	1.456(2)	C10—C11	1.386(2)
O3—C16	1.424(2)	C11—C12	1.390(2)
N1—C1	1.4474(19)	C12—C13	1.370(2)
N1—C8	1.3771(19)	C14—C15	1.467(3)
C1—C2	1.521(2)	C16—C17	1.455(4)
C2—C3	1.389(2)		

Bonding atoms	Bond angles (°)	Bonding atoms	Bond angles (°)
O4—S1—N2	106.55(9)	C7—C2—C1	119.66(14)
O4—S1—C11	107.66(7)	C7—C2—C3	119.06(16)
O5—S1—O4	119.32(9)	C4—C3—C2	119.85(19)
O5—S1—N2	106.24(9)	C5—C4—C3	120.63(19)
O5—S1—C11	108.67(8)	C6—C5—C4	119.99(19)
N2—S1—C11	107.91(7)	C5—C6—C7	119.8(2)
O1—P1—O2	114.80(8)	C2—C7—C6	120.68(18)
O1—P1—O3	114.84(9)	N1—C8—C9	123.67(13)
O1—P1—C1	113.18(7)	N1—C8—C13	117.85(13)
O2—P1—O3	106.72(9)	C9—C8—C13	118.44(13)
O2—P1—C1	105.04(8)	C10—C9—C8	120.24(14)
O3—P1—C1	100.89(7)	C9—C10—C11	120.26(14)
C14—O2—P1	124.21(14)	C10—C11—S1	121.50(12)
C16—O3—P1	124.47(15)	C10—C11—C12	120.03(14)
C8—N1—C1	123.58(13)	C12—C11—S1	118.44(11)
N1—C1—P1	105.77(10)	C13—C12—C11	119.90(14)
N1—C1—C2	115.66(13)	C12—C13—C8	121.11(14)
C2—C1—P1	114.24(10)	O2—C14—C15	110.7(2)
C3—C2—C1	121.28(15)	O3—C16—C17	110.1(2)

Table 6

Selected torision angles (°) of crystals **4a**.

Bonding atoms	Torsion angles	Bonding atoms	Torsion angles
S1—C11—C12—C13	−176.89(13)	N2—S1—C11—C10	−103.90(15)
P1—O2—C14—C15	−92.6(3)	N2—S1—C11—C12	74.23(15)
P1—O3—C16—C17	175.9(2)	C1—P1—O2—C14	−132.72(18)
P1—C1—C2—C3	−79.58(17)	C1—P1—O3—C16	168.9(2)
P1—C1—C2—C7	100.59(16)	C1—N1—C8—C9	−1.5(2)
O1—P1—O2—C14	−7.8(2)	C1—N1—C8—C13	176.24(14)
O1—P1—O3—C16	46.8(3)	C1—C2—C3—C4	179.12(17)
O1—P1—C1—N1	57.95(12)	C1—C2—C7—C6	179.94(17)
O1—P1—C1—C2	−173.69(11)	C2—C3—C4—C5	1.1(3)
O2—P1—O3—C16	−81.6(2)	C3—C2—C7—C6	0.1(3)
O2—P1—C1—N1	−176.07(11)	C3—C4—C5—C6	−0.2(3)
O2—P1—C1—C2	−47.71(13)	C4—C5—C6—C7	−0.8(3)
O3—P1—O2—C14	120.72(18)	C5—C6—C7—C2	0.8(3)
O3—P1—C1—N1	−65.27(12)	C7—C2—C3—C4	−1.1(3)
O3—P1—C1—C2	63.09(13)	C8—N1—C1—P1	−155.29(13)
O4—S1—C11—C10	10.74(16)	C8—N1—C1—C2	77.20(19)
O4—S1—C11—C12	−171.12(13)	C8—C9—C10—C11	−0.6(3)
O5—S1—C11—C10	141.29(14)	C9—C8—C13—C12	−1.0(2)
O5—S1—C11—C12	−40.57(15)	C9—C10—C11—S1	177.29(13)
N1—C1—C2—C3	43.6(2)	C9—C10—C11—C12	−0.8(2)
N1—C1—C2—C7	−136.25(16)	C10—C11—C12—C13	1.3(2)
N1—C8—C9—C10	179.24(15)	C11—C12—C13—C8	−0.3(3)
N1—C8—C13—C12	−178.92(15)	C13—C8—C9—C10	1.5(2)

Table 7

Hydrogen atom coordinates (Å × 10⁴) and isotropic displacement parameters (Å² × 10³) for **(4a)**.

Atom	x	y	z	U(eq)
H1	9163.12	3514.1	3213.16	46
H2A	5295.57	429.73	2308.07	58
H2B	6076.87	−237.97	2054.07	58
H1A	8054.74	5387.51	3166.79	37
H3	8330.03	3411.41	4280.16	57
H4	7311.74	3348.45	5044.91	73
H5	6071.88	4670.91	5155.43	74
H6	5843.84	6075.88	4505.76	69
H7	6887.63	6181.15	3748.57	53
H9	6774.01	4370.24	2865.86	44
H10	5746.71	3391.05	2269.28	45
H12	7872.46	1065.95	2009.18	44
H13	8890.3	2016.22	2608.89	44
H14A	9297.68	8347.29	3874.9	68
H14B	9932.55	7810.73	3399.4	68
H15A	10,535.47	7816.58	4497.21	129
H15B	10,899.58	8714.38	4063.46	129
H15C	11,179.29	7424.43	3994.7	129
H16A	11,212.02	5396.77	4313.79	99
H16B	11,462.27	4505.37	3850.77	99
H17A	10,824.82	3982.32	4908.83	145
H17B	11,875.44	3726.41	4667.76	145
H17C	10,953.36	3062.27	4445.27	145

Table 8

Docking score and binding energy (kcal/mol) of synthesized sulfamidophosphonates with the reference.

Compound code	Glide score	Binding energy
4a	−5.498	−58.548
4b	−6.138	−62.526
4c	−5.408	−62.168
4d	−5.523	−58.760
4e	**−6.388**	**−65.074**
4f	−4.802	−50.550
4 g	−5.485	−59.644
co-crystalized	−6.518	−47.112

Fig. 5. Validation of the docking protocol: docked and co-crystalized (methyl 4-sulfamoylbenzoate) in the SARS-CoV-2 main protease after self-docking calculation.
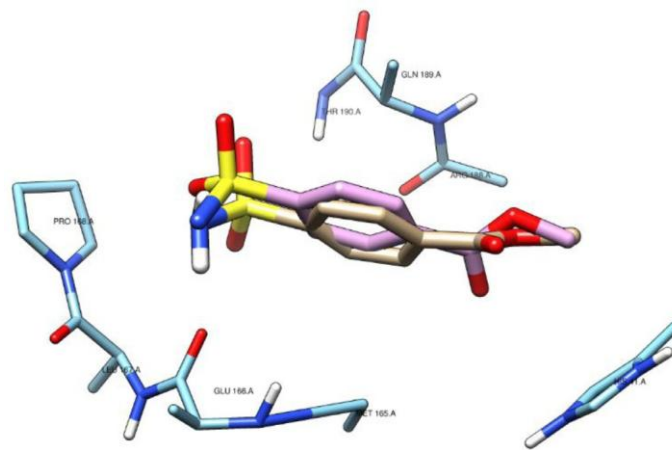
and prepared with Ligprep using Optimized Potentials for Liquid Simulation (OPLS3e) force field with a convergence of heavy atoms of 0.30 A° [31]. The Grid was centered on the centroid of the co-crystallized ligand (Methyl 4-sulfamoylbenzoate). The final prepared PDB file of the protein and synthesized sulfamidophosphonates (**4a, 4b, 4c, 4d, 4e, 4f**, and 4g) were submitted to run the docking process. Docking studies were conducted using Glide software [32] at Standard Precision (XP) [33]. Output files of Methyl 4-sulfamoylbenzoate and docked compounds along with SARS-CoV-2 main protease protein were visualized on Chimera software.

3.5. Molecular docking study

In order to understand the interactions between protein and ligand, a molecular docking study was performed to explore the binding mode of the prepared sulfamidophosphonates to the
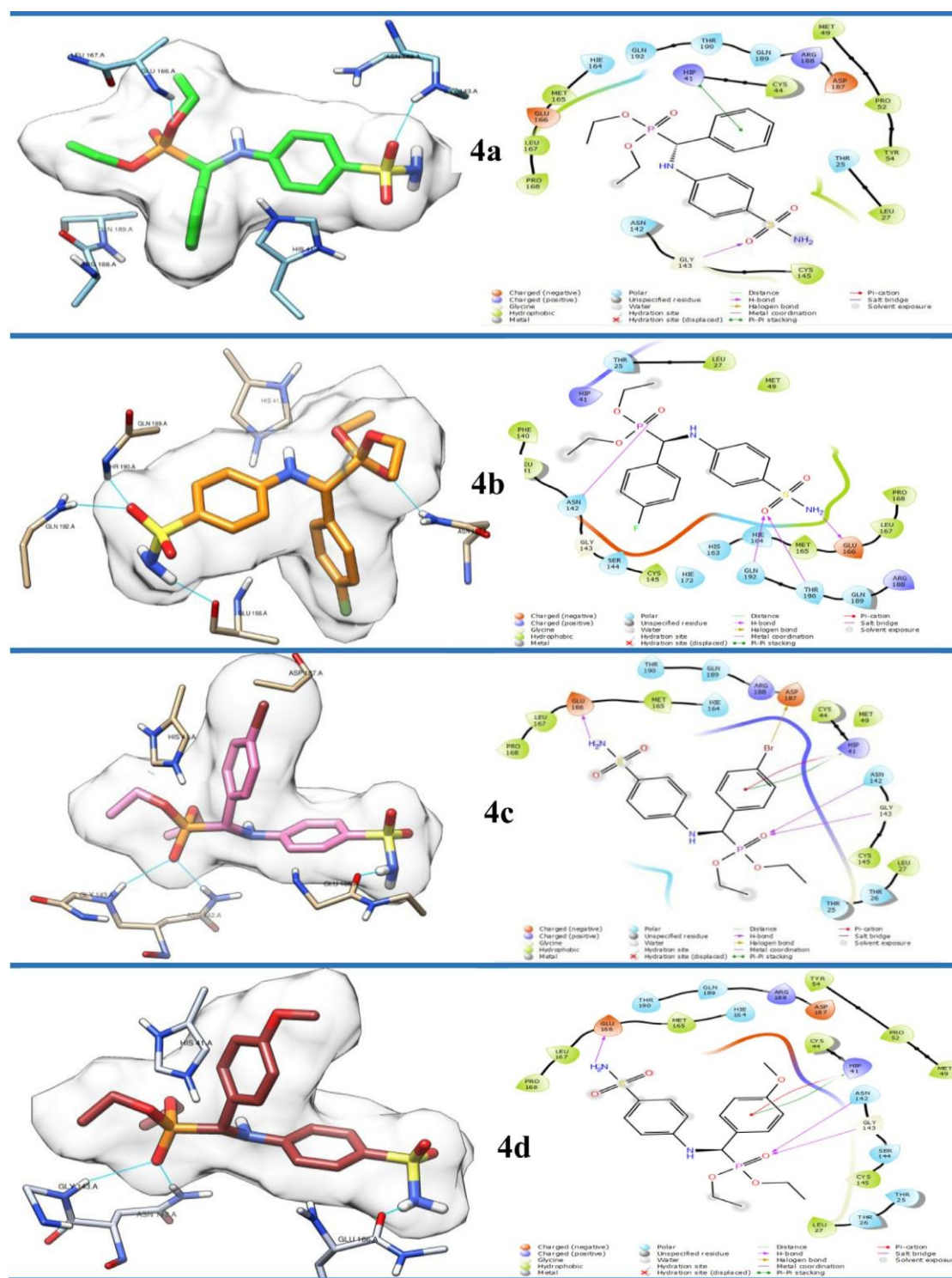
Fig. 6. 3D left and 2D right binding disposition of compounds **4a**, **4b**, **4c** and **4d** after docking calculations in the active site of SARS-CoV-2 main protease. The amino acid residues were shown as stick model and H-bonds were shown as cyan lines.

SARS-CoV-2 main protease. Our studies were realized using the Schrodinger suite (version 11.8) and UCSF Chimera (version 1.13.1) programs. The co-crystal (Methyl 4-sulfamoylbenzoate) was taken as a reference ligand to investigate the binding mode of the studied synthesized derivatives.

To validate the docking protocol, we re-dock the co-crystal (Methyl 4-sulfamoylbenzoate) in the active site of the SARS-CoV-2 main protease. (Fig. 5) shows docked Methyl 4-sulfamoylbenzoate and co-crystallized one in almost the same position among the re-

ceptor (RMSD value is 0.8412 < 1 Å) that confirmed validation of docking protocol.

The results of this study, showing the estimated glide score and bond energy of anchored positions, are presented in (Table 8). A molecular docking study of all compounds revealed compounds (**4a, 4b, 4c, 4d, 4e, 4f,** and 4g) found to be stable inside the cavity. All these Compounds **4a, 4b, 4c, 4d, 4e, 4f,** and 4g gave better binding energy and good glide score in the range (−50.550 to −65.074 kcal/mol), (−4.802 to −6.388 kcal/mol), respectively, when
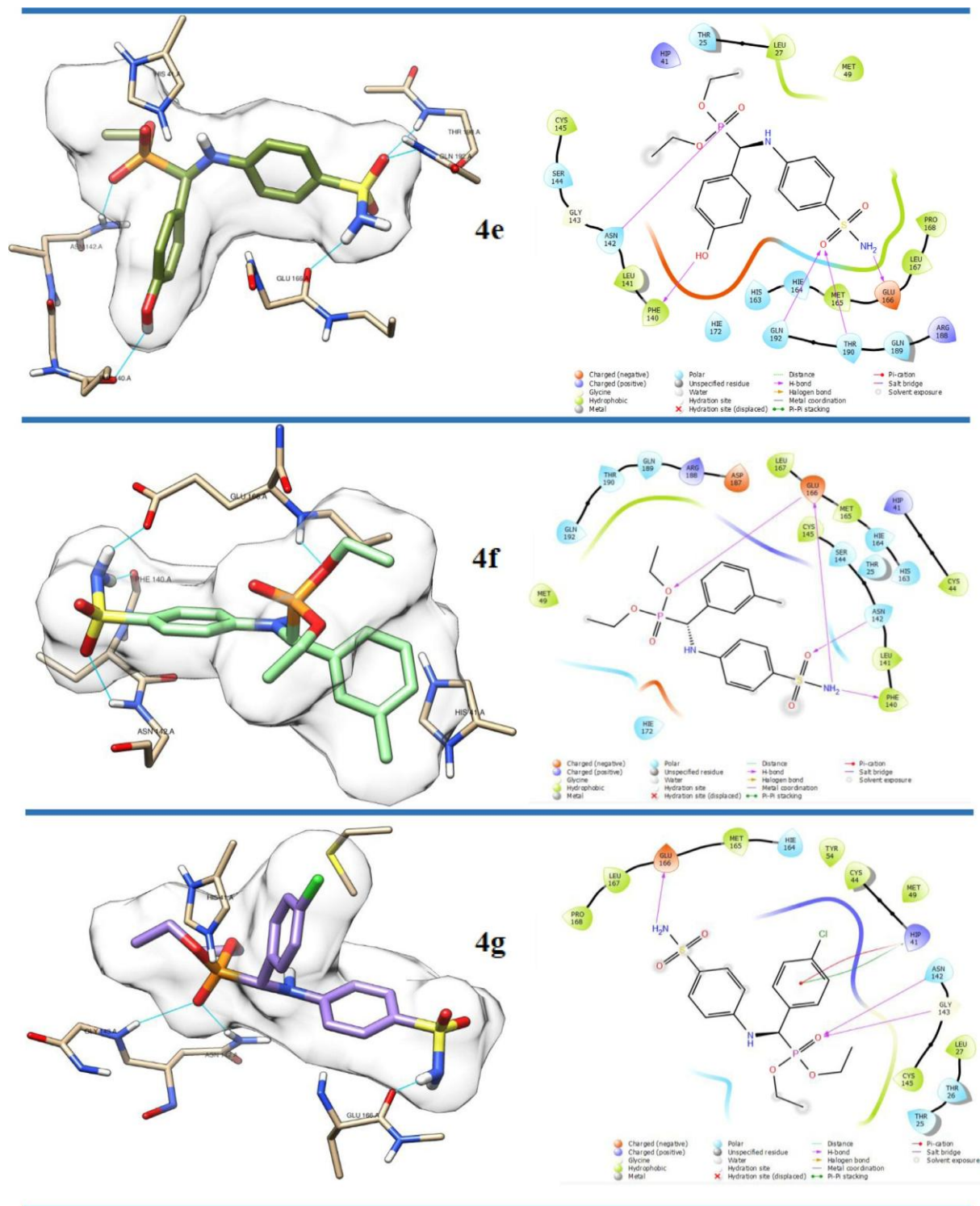
Fig. 7. 3D left and 2D right binding disposition of compounds **4e**, **4f** and **4g** after docking calculations in the active site of SARS-CoV-2 main protease. The amino acid residues were shown as stick model and H-bonds were shown as cyan lines.

compared with the reference compound, with a binding energy of 47.112 kcal/mol and docking score of −6.551 kcal/mol. We observed that all compounds form a hydrogen bond with the Glu166 residue as the binding of the reference ligand and other significant hydrogen bonds with other residues at the active site as Glu166, Tyr190, Asn142, Gln192, and Phe140. The compound **4e** is the most stable among the synthesized sulfamidophosphonates, which has the least binding energy −65.074 kcal/mol) and is the most favorable and good docking score (−6.388 kcal/mol), with the most valuable

interaction inside the pocket. This compound formed 5 hydrogen bonds (Fig. 7): the first one between the doublet of the nitrogen atom of the sulfamide group and Glu166 residue, the second between the doublet of the oxygen atom of the sulfamide group and Thr190 residue, the third between the same doublet of the oxygen atom of the sulfamide group and Gln192 residue, the fourth between the doublet of the oxygen atom of the hydroxyl group and Phe140, and the last between Asn142 residue and the doublet of the oxygen atom of the phosphonate group. Moreover, the

Table 9

Analysis of binding interaction (hydrogen bond and hydrophobic interaction) of synthesized sulfamidophosphonates with the reference compound against SARS-CoV-2 main protease.

Compound	Residues involved in hydrogen bond	Residues involved in hydrophobic interaction
4a	Glu166, Gly143	Met49, Met165, Leu27, Pro52, Cys145, Cys44, Pro168, Tyr54
4b	Glu166, Thr190, Gln192, Asn142	Met49, Met165, Leu27, Pro168, Cys145, Phe140, Leu167
4c	Glu166, Gly143, Asn142	Met49, Met165, Leu27, Cys145, Cys44
4d	Glu166, Gly143, Asn142	Met49, Tyr54, Pro52, Leu27, Cys145, Cys44
4e	Glu166, Tyr190, Asn142, Gln192, Phe140	Met49, Leu27, Cys145, Pro168
4f	Glu166, Asn142, Phe140	Met49, Met165, Cys145, Cys44
4 g	Glu166, Asn142, Gly143	Met49, Met165, Tyr54, Leu27, Cys145, Cys44

latter developed hydrophobic interactions with Met49, Leu27, Cys145, and Pro168 residues (Table 9), which explains the high value of its glide score and binding energy.

Also, compound **4b** show significant stability in the active site with binding energy higher than the reference ligand, this compound formed an important hydrogen bond with the Glu166 residue, as well as other hydrogen bonds with the Thr190, Gln192, and Asn142 residues (Fig. 6). Moreover, it developed hydrophobic interactions with Met49, Met165, Leu27, Pro168, Cys145, Phe140, and Leu167 residues (Table 9).

Compounds **4c** and **4d** formed the same hydrogen bonds inside the cavity with Glu166, Gly143, and Asn142, as well as a $\Pi-\Pi$ stacking interaction and a Π−cation interaction with Hip41 (Fig. 6), which explains the convergence of the glide score values −5.408 and −5.523 kcal/mol, respectively. The **3c** derivative thus developed five hydrophobic interactions with Met49, Met165, Leu27, Cys145, and Cys44, and the **4d** six with Met49, Tyr54, Pro52, Leu27, Cys145, and Cys44 (Table 9).

The last compound (**4f**) is the least stable compared to other compounds, its glide score is −4.802 kcal/mol and its binding energy is −50.550 kcal/mol, it formed 3 hydrogen bonds with Glu166, Asn142, and Phe140, the hydrophobic interactions are formed with Met49, Met165, Cys145 and Cys44 (Fig. 7).

Docking analysis revealed that all seven compounds interact satisfactorily with SARS-CoV-2 main protease and confirms the significant role of the donor and acceptor moieties such as phosphonate and sulfamide groups.

4. Conclusion

A new series of α-sulfamidophosphonates derivatives bearing sulfanilamide moiety were designed and synthesized. A one-pot synthetic strategy was developed via a three-component Kabachnik-Fields reaction starting from commercially available compounds. Docking analysis revealed that all seven compounds interact satisfactorily with the main protease of SARS-CoV-2 and thus confirm the significant role of donor and acceptor fragments such as phosphonate and sulfonamide groups. Moreover, higher docking scores and binding free energies were observed for the studied compounds compared to the ligand reference.

Declaration of Competing Interest

The authors declare that they have no known competing financial interests or personal relationships that could have appeared to influence the work reported in this paper.

CRediT authorship contribution statement

Rayenne Redjemia: Conceptualization, Methodology. **Malika Berredjem:** Conceptualization, Methodology, Writing − review & editing. **Ali Dekir:** Software, Visualization. **Malika Ibrahim-Ouali:** Supervision, Validation. **Mohamed Aissaoui:** Software, Visualization. **Sofiane Bouacida:** Formal analysis. **Abdeslem Bouzina:** Soft-ware, Visualization. **Rania Bahadi:** Conceptualization, Methodology.

Data availability

No data was used for the research described in the article.

Supplementary materials

Supplementary material associated with this article can be found, in the online version, at doi:10.1016/j.molstruc.2022.134602.

References

[1] Y.T. Tan, D.J. Tillett, I.A. McKay, Molecular strategies for overcoming antibiotic resistance in bacteria, Mol. Med. Today. 6 (2000) 309–314, doi:10.1016/S1357-4310(00)01739-1.

[2] J.B. Bremner, J.I. Ambrus, S. Samosorn, Dual action-based approaches to antibacterial agents, Curr. Med. Chem. 14 (2007) 1459–1477, doi:10.2174/092986707780831168.

[3] J. Chen, Y. Luo, S. Zhang, Z. Liang, Y. Wang, Y. Zhang, G. Zhou, Y. Jia, L. Chen, D. She, Community-acquired necrotizing pneumonia caused by methicillin-resistant Staphylococcus aureus producing Panton–Valentine leukocidin in a Chinese teenager: case report and literature review, Inter. J. Infect. Dis. 26 (2014) 17–21, doi:10.1016/j.ijid.2014.02.025.

[4] E.A. Grabsch, A.A. Mahony, D.R.M. Cameron, R.D. Martin, M. Heland, P. Davey, M. Petty, S. Xie, M.l. Grayson, Significant reduction in vancomycin-resistant enterococcus colonization and bacteraemia after introduction of a bleach-based cleaning-disinfection programme, J. Hosp. Infect. 82 (2012) 234–242, doi:10.1016/j.jhin.2012.08.010.

[5] Y. Chong, Y. Ito, T. Kamimura, S. Shimoda T. Miyamoto, K. Akashi H. Yakushiji, N. Shimono, Fatal candidemia caused by azole-resistant Candida tropicalis in patients with hematological malignancies, J. Infect. Chemother. 18 (2012) 741–746, doi:10.1007/s10156-012-0412-9.

[6] C.D. Wells, J.P. Cegielski, L.J. Nelson, K.F. Laserson, T.H. Holtz, A. Finaly, K.G. Gastro, K. Weyer, HIV infection and multidrug-resistant tuberculosis: the perfect storm, J. Infect. Dis. 196 (2007) 86–107, doi:10.1086/518665.

[7] P.G.D. Benedetti. In: Advances in Drug Research. B. Testa, editor. Academic Press. London and New York; 16 (1987) 227–279.

[8] M.J. Mengelers, P.E. Hougee, L.H. Jansson, A.S. Van Miert, Structure-activity relationship between antibacterial activities and physicochemical properties of sulfonamides, J. Vet. Pharmacol. Therap. 20 (1997) 276–283, doi:10.1046/j.1365-2885.1997.00063.x.

[9] F. Zani, P. Vicini, Antimicrobial activity of some 1,2-Benzisothiazoles having a Benzenesulfonamide Moiety, Arch. Pharm. Pharm. Med. Chem. 331 (1999) 219–223 6%3C219::AID-ARDP219%3E3.0.CO;2-U, doi:10.1002/(SICI)1521-4184(199806)331.

[10] B. Zhang, X.T. Hu, J. Gu, Y.S. Yang, Y.T. Duan, H.L. Zhu, Discovery of novel sulfonamide-containing aminophosphonate derivatives as selective COX-2 inhibitors and anti-tumor candidates, Bioorg. Chem. 105 (2020) 104390–104400, doi:10.1016/j.bioorg.2020.104390.

[11] C. Verma, A. Singh, G. Pallikonda, M. Chakravarty, M.A. Quraishi, I. Bahadur, E.E. Ebenso, Aryl sulfonamidomethylphosphonates as new class of green corrosion inhibitors for mild steel in 1 M HCl: electrochemical, surface and quantum chemical investigation, J. Mol. Liq. 209 (2015) 306–319, doi:10.1016/j.molliq.2015.06.013.

[12] S. Bhagat, M. Supriya, S. Pathak, D. Sriram, A.K. Chakraborti, α-Sulfonamidophosphonates as new anti-mycobacterial chemotypes: design,

development of synthetic methodology, and biological evaluation, Bioorg. Chem. 82 (2018) 246–252, doi:10.1016/j.bioorg.2018.09.023.

[13] M.D. Segall, A.P. Beresford, J.M.R. Gola, D. Hawksley, M.H. Tarbit, Focus on success: using a probabilistic approach to achieve an optimal balance of compound properties in drug discovery, Expert Opin. Drug Metab. Toxicol. 2 (2006) 325–337, doi:10.1517/17425255.2.2.325.

[14] S.P. Adhikari, S. Meng, Y.J. Wu, Y.P. Mao, R.X. Ye, Q.Z. Wang, C. Sun, S. Sylvia, S. Rozelle, H. Raat, H. Zhou, Epi- demiology, causes, clinical manifestation and diagnosis, prevention and control of coronavirus disease (COVID-19) during the early outbreak period: a scoping review, Infect. Dis. Poverty 9 (2020) 1–12, doi:10.1186/s40249-020-00646-x.

[15] A.M. Kanhed, D.V. Patel, D.M. Teli, N.R. Patel, M.T. Chhabria, M. Ram, Identification of potential Mpro inhibitors for the treatment of COVID–19 by using systematic virtual screening approach, Mol. Divers. 25 (2021) 383–401, doi:10.1007/s11030-020-10130-1.

[16] V.A. Obakachi, N.D. Kushwaha, B. Kushwaha, M.C. Mahlalela, Design and synthesis of pyrazolone-based compounds as potent blockers of SARS-CoV-2 viral entry into the host cells, J. Mol. Struct. 1241 (2021) 130665–130680, doi:10.1016/j.molstruc.2021.130665.

[17] S.P. Negi, P.A. Chawla, A. Faruk, V. Chawla, Role of heterocyclic compounds in SARS and SARS CoV-2 pandemic, Bioorg. Chem. 104 (2020) 104315–104350, doi:10.1016/j.bioorg.2020.104315.

[18] M. Chalkha, A. Nakkabi, T.B. Hadda, M. Berredjem, A. El Moussaoui, M. Bakhouch, M. Saadi. L. El Ammari, F.A. Almalki, H. Laaroussi, V. Jevtovic, M. El Yazidi, Crystallographic study, biological assessment and POM/Docking studies of pyrazoles-sulfonamide hybrids (PSH): identification of a combined Antibacterial/Antiviral pharmacophore sites leading to *in-silico* screening the anti-Covid-19 activity, J. Mol. Struct. 1267 (2022) 133605–133628, doi:10.1016/j.molstruc.2022.133605.

[19] A. Scozzafava, T. Owa, A. Mastrolorenzo, C.T. Supuran, Anticancer and antiviral sulfonamides, Curr. Med. Chem. 10 (2003) 925–953, doi:10.2174/0929867033457647.

[20] F. Helgstrand, B. Eriksson, N.G. Johanssonb, B. Lannero, A. Larsson, A. Misiorny, J.O. Noren, B. Sjoberg, K. Stenberg, G. Stening, S. Stridh, B. Oberg, S. Alenius, L. Phlilipson, Trisodium phosphonoformate, a new antiviral compound, J. Sci. 201 (1978) 819–821, doi:10.1126/science.210500.

[21] O.V. Dolomanov, L.J. Bourhis, Gildea R.J, J.A.K. Howard, H. Puschmann, OLEX2: a complete structure solution, refinement and analysis program, J. Appl. Cryst. 42 (2009) 339–341, doi:10.1107/S0021889808042726.

[22] G.M. Sheldrick, N.K. Sebbar, M. Ellouz, E.M. Essassi, Y. Ouzidan, J.T. Mague, Crystal structure of 4-benzyl-2H-benzo[b][1,4]thia-zin-3(4H)-one, Acta Cryst. 71 (2015) 3–8 10.1107%2FS2056989015022276.

[23] L.J. Farrugia, WinGX and ORTEP for Windows: an update, J. Appl. Cryst. 45 (2012) 849–854, doi:10.1107/S0021889812029111.

[24] K. Bechlem, M. Aissaoui, B. Belhani, K. Otmane Rachedi, S. Bouacida, R. Bahadi, S.-.E. Djouad, R. Ben Mansour, M. Bouaziz, F. Almalki, T. Ben Hadda, M. Berredjem, Synthesis, X-ray crystallographic study and molecular docking of new *α*-sulfamidophosphonates: POM analyses of their cytotoxic activity, J. Mol. Struct. 1210 (2020) 127990–127997, doi:10.1016/j.molstruc.2020.127990.

[25] [a] B. Belhani, M. Berredjem, M. Le Borgne, Z. Bouaziz, J. Lebreton, N.-E. Aouf, A one-pot three-component synthesis of novel *α*-sulfamidophosphonates under ultrasound irradiation and catalyst-free conditions, RSC. Adv. 5 (2015) 39324–39329, doi:10.1039/C5RA03473F; [b] B. Belhani, A. Bouzina, M. Berredjem, N.-E. Aouf, One-pot synthesis of novel oxazaphosphinanes under ultrasound irradiation and solvent-free conditions, Monatshefte Chem.-Chem. Monthly 146 (2015) 1871–1875, doi:10.1007/s00706-015-1461-4.

[26] M. Guerfi, M. Berredjem, A. Bouzina, T.B. Hadda, C. Marminon, K.O. Rachedi, Novel *α* -sulfamidophosphonate analogues of fotemustine: efficient synthesis using ultrasound under solvent-free conditions, Monatshefte Chem. - Chem. Monthly 151 (2020) 1859–1865, doi:10.1007/s00706-020-02711-5.

[27] [a] S.-E. Djouad, M. Berredjem, F-Z.Hadjadj Aoulc, F. Bouchareb, M. Guerfi, T.B. Hadda, M. Aissaoui, B. Belhani, *In silico* drug design and molecular docking of novel Amidophosphonates and sulfamidophosphonates as inhibitors of urokinase-type plasminogen activator, J. Indian Chem. Soc. 99 (2022) 100650–100663, doi:10.1016/j.jics.2022.100650; [b] S.G. Lakoud, M. Berredjem, N.-E. Aouf, Efficient method for the synthesis of *α*-Amidophosphonates via the Michaelis-Arbuzov reaction, Phosphorus Sulfur Silicon Relat. Elem. 187 (2012) 762–768, doi:10.1080/10426507.2011.645173.

[28] [a] W. Boufas, H. Cheloufi, F. Bouchareb, M. Berredjem, N.-E. Aouf, Convenient synthesis of novel N -acylsulfonamides containing phosphonate moiety, Phosphorus. Sulfur Silicon Relat. Elem. 190 (2015) 103–111, doi:10.1080/10426507.2014.931398; [b] R. Bouasla, M. Berredjem, N.-.E. Aouf, C. Barbey, 1,2,3,4-Tetrahydroisoquinoline-2-sulfonamide, Acta Crystallogr. E 64 (2008) 432–439, doi:10.1107/S1600536807068158.

[29] H. Cheloufi, M. Berredjem, W. Boufas, F. Bouchareb, A. Djahoudi, N.-.E. Aouf, Efficient synthesis, characterization, and antibacterial activity of novel N-acylsulfonamides and sulfonylureas, phosphorus, Sulfur Silicon Relat. Elem 189 (2014) 1396–1404, doi:10.1080/10426507.2013.865125.

[30] A. Douangamath, D. Fearon, P. Gehrtz, T. Krojer, P. Lukacik, C.D. Owen, E. Resnick, C. Strain-Damerell, A. Aimon, P. Ábrányi-Balogh, J. Brandão-Neto, A. Carbery, G. Davison, A. Dias, T.D. Downes, L. Dunnett, M. Fairhead, J.D. Firth, S.P. Jones, A. Keeley, G.M. Keserü, H.F. Klein, M.P. Martin, M.E.M. Noble, P. O'Brien, A. Powell, R.N. Reddi, M. Snee, M.J. Waring, C. Wild, N. London, F. von Delft, M.A. Walsh, Crystallographic and electrophilic fragment screening of the SARS-CoV-2 main protease, Nat. Commun. 11 (2020) 5047–5058, doi:10.1038/s41467-020-18709-w.

[31] S. Release, LigPrep, Version 3.4, Schrödinger, 2, LLC, New York, NY, 2015.

[32] R.A. Friesner, J.L. Banks, R.B. Murphy, T.A. Halgren, J.J. Klicic, D.T. Mainz, M.P. Repasky, E.H. Knoll, D.E. Shaw, M. Shelley, J.K. Perry, P. Francis, P.S. Shenkin, Glide: a new approach for rapid, accurate docking and scoring. 1. Method and assessment of docking accuracy, J. Med. Chem. 47 (2004) 1739–1749, doi:10.1021/jm0306430.

[33] R.A. Friesner, R.B. Murphy, M.P. Repasky, L.L. Frye, J.R. Greenwood, T.A. Halgren, D.T. Mainz, Extra precision glide: docking and scoring incorporating a model of hydrophobic enclosure for protein-ligand complexes, J. Med. Chem. 49 (2006) 6177–6196, doi:10.1021/jm051256o.